Pore fabric anisotropy: testing the equivalent pore concept using magnetic measurements on synthetic voids of known geometry

Sebastian Jones[1], Philip Benson[1,2*] and Philip Meredith[1]

[1]Mineral, Ice and Rock Physics Laboratory, Department of Earth Sciences, University College London, London WC1E 6BT, UK

[2]Lassonde Institute, University of Toronto, 170 College Street, Toronto, Ontario M5S 3E3, Canada.

Accepted 20/03/2006; Received 20/10/2005; in original form 24/10/2005

Abbreviated title: **Pore fabric anisotropy**

*Philip M Benson
Dept. Earth Sciences
University College London
Gower Street
London
WC1E 6BT
U.K.
Tel. +1 416 978 1276
Fax. +44 7679 2685
p.benson@ucl.ac.uk

Abstract/Summary

We present an experimental and modelling study of pore fabric anisotropy using the method of anisotropy of magnetic susceptibility (AMS) applied to synthetic void spaces of known dimensions saturated with a high susceptibility magnetic ferrofluid. We analysed the data using the equivalent pore concept (EPC) proposed by Hrouda et al. (2000), who consider the theoretical demagnetization factors of an ellipsoid in order to relate physical pore fabric to magnetic measurements of lineation, foliation and bulk anisotropy. To test this theory, synthetic samples were prepared from cylindrical polycarbonate blanks, 25mm in diameter by 22mm long. A variety of 'special fabrics' were prepared by machining internal void spaces of: (a) a quasi-spherical fabric comprising a cylinder 10mm in diameter by 8.8mm long, (b) a capillary-like fabric comprising a set of 19 equally spaced holes, (c) a bedding-like fabric comprising a linear row of five larger diameter holes, and (d) a crack-like fabric comprising a stack of four penny-shaped voids. A second set of quasi-spheroidal fabrics were prepared by machining a hemispherical cutter to different depths into the blanks. Eight samples were prepared with principal axial to radial axis ratios (a/r) from 0.75 to 1.3 (i.e. from oblateness through sphericity to prolateness). With the exception of the quasi-spherical fabric, the 'special fabrics' exhibit high anisotropy, with a maximum foliation of 1.41 and a maximum lineation of 1.29. Using a ferrofluid with a fixed intrinsic susceptibility of 1.09 SI, the quasi-spheroidal shape effect is investigated with change in value of the a/r ratio. As the a/r ratio increases, foliation decreases and lineation increases, reflecting the change from an oblate to a prolate fabric. The EPC is then used to estimate the physical void anisotropy from the magnetic measurements of lineation and foliation for direct comparison with the known geometry. Overall, the EPC method makes a reasonable job of estimating the void geometry, but it underestimates the physical void anisotropy by an average of about 8%. We therefore report the effect of varying the intrinsic susceptibility of the ferrofluid on a void with a constant a/r ratio of 1.2. As ferrofluid concentration is increased, the EPC predicted void geometry converges to the known physical void geometry. However, even for the highest intrinsic susceptibility ferrofluid used (3.34 SI) the EPC under-predicts the known void anisotropy. We therefore propose a simple, empirical correction factor that allows the EPC method accurately to predict real physical void space anisotropy from AMS measurements.

Key words: Anisotropy, Demagnetization, Induced magnetization, Inhomogeneous media, Laboratory measurement, Magnetic susceptibility, Porosity

Introduction

Porosity is a ubiquitous feature of crustal rocks. However, the mechanisms responsible for porosity evolution are diverse, ranging from depositional processes such as sedimentary sorting and grain alignment, through diagenetic processes such as compaction and cementation, petrogenetic processes such as thermal cracking (due to cooling or heating), to deformational processes such as microcracking caused by differential stress. The porosity that evolves from the superposition of these processes over time may therefore exhibit a complex geometry or fabric. In particular many of these processes, such as grain sorting, compaction and microcracking, have an inherent directionality which may lead to anisotropy of the void space. This is important, since the void space of rock, and its geometry, is a key control on other mechanical and physical properties (e.g. Lo et al., 1986; Jones and Meredith, 1998; Rasolofosaon and Zinszner, 2002; Benson, 2004; Benson et al., 2005; Louis et al., 2005).

Under these circumstances, the classical definition of porosity as a volume-averaged, scalar quantity is not adequate fully to quantify the geometry of the void space that constitutes that porosity. However, a number of techniques have been proposed that aim directly to measure void space geometry. One effective method is to measure the anisotropy of magnetic susceptibility (AMS) of pore space saturated with magnetic ferrofluid (Pfleiderer and Halls, 1990, 1994; Pfleiderer and Kissel, 1994; Hrouda et al., 2000; Benson et al., 2003; Benson, 2004). In order to avoid ambiguity, Benson et al. (2003) named this the pore-space AMS (pAMS) technique in order to distinguish it from the more traditional technique used to measure the magnetic fabric of a dry rock matrix (Tarling and Hrouda, 1993), which they named matrix AMS (mAMS).

The mAMS technique has become a commonly used tool for measuring the grain fabric in sedimentary rocks containing magnetic minerals, and hence for inferring details of depositional processes and palaeocurrent directions. In principle, it is necessary to determine the dry matrix AMS prior to using the pAMS technique to determine void space anisotropy. Following mAMS measurements, the samples pore space is saturated with a high susceptibility magnetic ferrofluid to provide it with a high artificial susceptibility (Figure 1). The measured total AMS now reflects the superposition of the AMS of the dry matrix (mAMS) and that of the ferrofluid saturated void space (pAMS). The pAMS can then be recovered simply by subtracting the mAMS data from the total AMS data on a measurement by measurement basis. In practice, however, for high porosity rocks the mAMS measurements are often 3 orders of magnitude or more lower than the pAMS measurements and can effectively be neglected (Benson et al., 2003).

A major advantage of the pAMS technique is that it can provide a true 3-D measure of the pore space anisotropy from measurements on a single core taken in any orientation relative to the principal anisotropy directions. Since AMS measurements constitute a second rank tensor, a magnetic anisotropy ellipsoid can be constructed, in which the orientations of the major, intermediate and minor axes represent the principal anisotropy direction, providing sufficient measurements are taken.

The equivalent pore concept

In principle, it is possible to relate the measured magnetic anisotropy to the physical void space anisotropy. In general, we find that the principal magnetic anisotropy directions

are closely coincident with the principal anisotropy directions of the overall void space (e.g. Pfleiderer and Halls, 1993; Benson et al., 2003). However, a significant problem arises in that the ratios of the lengths of the major, intermediate and minor axes of the measured susceptibility ellipsoid commonly underestimate the actual physical anisotropy of the void space. This arises due to an internal opposing magnetization induced by the applied measuring field; known as the "demagnetising factor" (Collinson, 1983).

The lengths of the three principal axes of the susceptibility ellipsoid are given by k_1, k_2 and k_3 respectively; with $k_1>k_2>k_3$. The magnetic anisotropy factors of lineation (L_m), foliation (F_m) and bulk anisotropy (P_m), as used in conventional palaeomagnetic work, are simply defined as the ratios of the lengths of these axes; with $L_m = k_1/k_2$, $F_m = k_2/k_3$, and $P_m = k_1/k_3$. Now consider an ellipsoid with principal axis lengths of a, b and c (where a>b>c) that represents the overall geometry of the physical void space anisotropy, as shown in Figure 2. While the principal anisotropy directions are the same, the lengths of the principal axes are different due to the demagnetization effect. In turn, this means that the magnetic anisotropy factors are not the same as those of the physical void space; i.e. $k_1/k_2 \neq a/b$; $k_2/k_3 \neq b/c$; and $k_1/k_3 \neq a/c$, or $L_m \neq L_v$, $F_m \neq F_v$ and $P_m \neq P_v$.

Nevertheless, we would still like to be able to use the magnetic measurements (which are relatively easy to measure) to provide us with quantitative information about the anisotropy of the physical void space (which is difficult or impossible to measure directly). The approach taken is to model an overall physical void space shape and alignment that would produce the same magnetic anisotropy parameters as the measured sample, taking the demagnetization effect into account. If this can be done, then a direct comparison can be made between the ellipsoid describing the pAMS data and that describing the average

physical void space. Such an analysis was first proposed by Hrouda et al. (2000) and is known as the *equivalent pore concept (EPC)*.

First, consider the shape effect on the AMS of a magnetic grain or magnetic fluid filled pore (Uyeda 1963; Hrouda et al., 2000):

(1)

where: $k_1>k_2>k_3$ are the principal susceptibilities,

$N_1>N_2>N_3$ are the demagnetising factors along those axes.

K_i denotes the intrinsic susceptibility, which is related to the measured susceptibility (K_m) via:

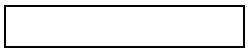

(2)

where, N = 1/3 is the demagnetising factor of a sphere.

The intrinsic susceptibility of a material is that value of susceptibility that would be obtained if no demagnetising factor acted internally to reduce the measured susceptibility as a result of the magnetic dipoles which are set up at the edges of the material (Collinson, 1983). For ellipsoidal geometries, the demagnetising factors can be derived exactly as a function of the physical principal axis lengths (a > b > c), and are given by Osborn (1945) as:

(3)

(4)

(5)

where the following parameters are also defined by Osborn (1945):

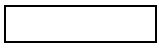

$(0<\theta<\pi/2)$

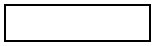

$(0<\varphi<\pi/2)$

$(0<\alpha<\pi/2)$

In equations 3, 4 and 5, F(n, θ) and E(n, θ) are elliptical integrals of the first and second kind, respectively, n is the integral modulus, and θ is the integral amplitude. Unfortunately, the elliptical integrals in these expressions mean that they cannot easily be re-arranged for direct substitution into equation 1. In this work, we solve these equations numerically using a MATLAB™ routine that calculates the value of elliptical integrals via the method provided by Zhang and Jin (1996); hence the demagnetising factor for any input value of a/b and b/c can then be computed. The accuracy of our routine was validated against original tabulated data from Osborn (1945), with which it agreed to 6 decimal places. To allow us to reverse this process, and determine values of a/b and b/c from input magnetic parameters, the approach of Hrouda et al. (2000) is again used. Values of lineation and foliation are calculated for a family of 'j' ellipsoids of principal axis lengths $a_j>b_j>c_j$ (where j=1,2,3…N; typically N=1000 is used for accuracy). The relative dimensions of a_j/b_j and b_j/c_j are then used to calculate the relative demagnetising factors, and hence the susceptibility

ratios $L_m = k_1/k_2$ and $F_m = k_2/k_3$ via equations 1 to 5. The end result is an *equivalent pore* which produces the same magnetic lineation and foliation as the measured sample by taking into account the demagnetising factor produced by the presence of the ferrofluid in the void space. The calculated values of L_m and F_m are then superimposed on a grid of physical void lineation and foliation (the families of a_j/b_j and b_j/c_j), which represent the physical void geometry. The result is a set of Flinn charts (Flinn, 1962; Benson et al., 2003) as shown in Figure 3. Using such charts, we are able to read off the EPC predicted values of a/b (L_v) and b/c (F_v) for any given set of experimentally measured values of L_m and F_m pairs, and for any known ferrofluid intrinsic susceptibility.

However, earlier work, in which both pAMS and elastic wave velocity anisotropy measurements were made on samples of porous sandstones (Benson et al., 2003; Benson, 2004), suggested that the EPC methodology did not always fully compensate for the demagnetization effect. Unfortunately, it is not possible to test the EPC directly on samples of real rocks because we do not have an independent quantitative measure of void space and its anisotropy. Hence, in this study we have manufactured synthetic samples with known and controlled void geometries, allowing us directly and quantitatively to evaluate the effectiveness of the EPC technique.

Experimental method

Synthetic samples were prepared by machining different void space geometries into 25mm diameter by 22mm long polycarbonate cylinders (corresponding to the standard sample length/diameter ratio of 0.88 used in palaeomagnetic studies). Polycarbonate was chosen

because it possesses a very low magnetic susceptibility (approximately 85 $x10^{-6}$ SI), and it is not susceptible to residual stress cracking when voids are machined into it.

First, the set of special anisotropic fabrics illustrated in Figure 4 were prepared: (a) a quasi-spherical fabric comprising a single cylinder, 10mm in diameter by 8.8mm long, (b) a bedding-like fabric comprising a row of 5 holes, 3.3mm in diameter by 16mm long, (c) a capillary-like fabric comprising a set of 19 equally spaced holes, 2mm in diameter by 12mm long; and (d) a crack-like fabric comprising a tier of four penny-shaped voids, 18mm in diameter by 1.4mm thick. These geometries were specifically designed so that their internal volumes were approximately the same, so that their bulk susceptibilities, when filled with ferrofluid, would also be approximately the same. This is important to negate any possible influence of variation in bulk susceptibility on the measurements. Second, a spherical void and the set of six quasi-spheroidal voids illustrated in Figure 5 were prepared by machining hemispherical cutters to different depths into half samples. The half samples were then glued together to produce the finished samples. With the exception of the sphere the voids are therefore not true spheroids, but approximate that geometry to within 5%. The seven samples were prepared with axial to radial axis ratios (a/r) of: 0.75, 0.83, 0.92, 1.0, 1.1, 1.2, and 1.3 (i.e. from oblateness through sphericity to prolateness).

Following manufacture the synthetic voids were filled with EMG-905 ferrofluid (Ferrotec UK Ltd.) using a hypodermic syringe inserted through a 2 mm hole drilled axially from the top surfaces of samples into each void space. Great care was taken to ensure that the ferrofluid only reached the base of the filling holes in order that the hole does not affect the accuracy of measurement. This was achieved by simply sealing the top of the hole so that the ferrofluid is restricted to the void by a combination of surface tension and air pressure within

the hole. The surface tension of the ferrofluid is then sufficient to prevent capillary flow up the injection hole, even when the sample was rotated. The magnetic ferrofluid comprises a suspension of magnetically permeable nano-particles of magnetite in a carrier fluid. In order to vary the fluid concentration for this study, the ferrofluid was diluted with varying quantities of additional carrier fluid (Multipar H, Multisol Ltd.).

The anisotropy of magnetic susceptibility was then measured using a Kappabridge KLY-2 magnetic susceptibility bridge (AGICO Instruments). Samples were sequentially rotated into 15 different orientations in three dimensions, with a measurement made in each orientation. A least squares routine was then used to fit a magnetic susceptibility ellipsoid to the data (Jelinek, 1978). The average bulk susceptibility of the ferrofluid saturated voids was about 20 x 10^{-3} SI, so that the background susceptibility of the polycarbonate sample material represented only about 0.4% of the total. The same instrument was used to measure the susceptibility of the ferrofluid (K_m), via a method similar to that described by Hrouda et al. (2000). A small cylindrical well, approximately 3mm in diameter by 2.6mm deep, was filled with ferrofluid. As before, this shape is deliberately chosen to mimic the demagnetising properties of a sphere. For undiluted fluid, the average measured susceptibility for 10 readings was $1.580 \pm 0.014 \times 10^{-6}$ SI, corresponding to an intrinsic susceptibility of $K_i = 3.34$. This is in excellent agreement with identical measurements made by others on the same EMG-905 ferrofluid (Hrouda et al., 2000) where a value of $1.658 \pm 0.004 \times 10^{-6}$ SI was measured (corresponding to $K_i = 3.707$).

Results and Discussion

We have investigated the ability of the equivalent pore concept (EPC) theory to compensate measured pAMS data for the demagnetization effect in magnetic ferrofluid and thus allow accurate prediction of void space geometry. We have approached the investigation in three different but interlinked ways: first, through a qualitative study of different void geometries and fabrics (the geometry effect); second, through a quantitative study of quasi-spheroidal voids of known but different shapes (the shape effect); and third, through a quantitative study using ferrofluids of different intrinsic susceptibilities (the concentration effect).

Geometry Effect

A qualitative investigation of a range of special pore fabrics that are idealized versions of fabrics found in real rocks was performed to determine their effect on magnetic susceptibility anisotropy. Figure 6A shows a Flinn plot of the results of pAMS measurements on all the synthetic void geometries tested. All measurements were made using ferrofluid with an intrinsic susceptibility of 1.09 SI (50% concentration).

In principle, AMS studies of rocks (whether on the grain matrix or ferrofluid saturated pore space) should use spherical samples. This is impracticable in most cases. Instead, a cylindrical sample with a standard length/diameter ratio of 0.88 is used, since this ratio is considered the best approximation to a sphere (Porath et al., 1966). However, the measuring instrument (Kappabridge KLY-2) does not see the specimen as a geometrical whole, but simply the sum of the individual magnetic particles within the specimen. In this case, the external shape of the specimen becomes less important. Our measurements confirm this, since the pAMS data for the 10mm x 8.8mm cylindrical void plotted very close to the origin in the Flinn plot.

In contrast, the crack-like void space exhibited a high foliation of 1.41 with no lineation and the capillary-like void space exhibited a high lineation of 1.29 with no foliation. These values are also broadly consistent with the relative aspect ratios of the individual voids that make up the fabrics. The distribution of void space in the bedding-like sample produces a result that effectively combines the features of the two previous samples, with a high lineation due to the shape of each individual capillary, and a high foliation due to the five capillaries being arranged in a plane. Overall, the results show that the pAMS technique is very good at detecting the spatial distribution of the void space that contributes to the measured anisotropy parameters (i.e. lineation and foliation). This is true even when, as in these measurements, the total void space volume is the same in each sample.

Shape Effect

We have then expanded the investigation to a quantitative consideration of a set of synthetic quasi-spheroidal voids with axial to radial axis ratios ranging from 0.75 to 1.3 (from oblate to prolate). Figure 6B shows an expanded view of the pAMS results for the quasi-spheroidal samples. As expected, the prolate quasi-spheroids exhibit increasing lineation with increasing prolateness and no foliation, while the oblate quasi-spheroids exhibit increasing foliation with increasing oblateness and no lineation. Note, however, that in each case the value of the measured magnetic lineation or foliation is much lower than the actual geometric anisotropy of the voids. The spherical void plotted very close to the origin, again as expected.

We now apply the EPC theory to the magnetic measurements on the quasi-spheroids shown in Figure 6B using an intrinsic susceptibility of 1.09 SI for the ferrofluid. The results are shown in Figure 7 where both the measured magnetic anisotropy and the EPC calculated

void anisotropy are plotted against the actual physical anisotropy of the voids. Overall, application of the EPC method appears to correct the measured magnetic data very well and, hence, provide a reasonable estimate of the real void anisotropy. A least squares fit to the EPC corrected data yields $(a/r)_{EPC} = 0.978\ (a/r)_V + 0.011$, giving an average error of about 8% over the range studied. However, the use of the EPC still represents a very significant improvement over the raw, uncorrected AMS data (Figure 7). This improvement is especially noteworthy since it includes the error introduced by applying the theoretical demagnetising factors for ellipsoids to the quasi-spheroids used in our study (as noted earlier, the error between our machined quasi-spheroids and true spheroids is up to 5% by volume).

Concentration Effect

All the measurements reported in the previous section were made using a constant fluid concentration of 50%; corresponding to an intrinsic susceptibility of 1.09 SI. However, in order fully to evaluate the EPC method, we need to study the effect of ferrofluid concentration. The reason for this can be seen in the data of Figure 8A. Measured susceptibility (K_m) is not a linear function of the intrinsic susceptibility (K_i) of the fluid; rather, these parameters are related via the expression $K_m=K_i/(1+K_i/3)$ (Uyeda et al., 1963; Hrouda et al., 2000). This non-linearity is important because ferrofluids of widely different concentrations, and therefore different intrinsic susceptibilities, are commonly used in rock physics measurements due to the wide range of porosities found in natural rocks. For example, Figure 8B shows the theoretical magnetic lineation produced by five different ferrofluid concentrations for three different ellipsoidal void shapes. Different fluid concentrations produce large variations in the predicted magnetic lineation. Furthermore, we note a clear discrepancy in Figure 3 between a spherical pore geometry as measured by AMS (annotated $L_m = F_m$) and calculated via the EPC (annotated $L_v = F_v$) as a function of ferrofluid

concentration. Hence, before we can be confident of applying the EPC method in a robust way, we need to test whether it can account for variations in concentration.

We have therefore made pAMS measurements using ferrofluids of 5 different concentrations (5%, 10%, 20%, 50%, and 100%) on the same sample (the prolate quasi-spheroid with a/r = 1.2; Figure 5c). The results of the pAMS measurements are shown in Figure 9, together with the EPC calculated void anisotropy. As the intrinsic fluid susceptibility (concentration) is increased, the measured pAMS lineation increases linearly, but always grossly underestimates the true physical void anisotropy. This is exactly as expected, given the relationship between intrinsic and measured susceptibilities illustrated in Figure 8. However, the EPC calculated void anisotropy increases very non-linearly with increasing intrinsic susceptibility. At low concentrations, the EPC predicted anisotropy, although an improvement on the pAMS measured value, still grossly underestimates the physical anisotropy. However, this discrepancy decreases as concentration increases and the EPC predicted anisotropy approaches the true physical anisotropy asymptotically. At the highest concentration used (intrinsic susceptibility of 3.34 SI), the pAMS measured lineation is 1.111 and the EPC predicted anisotropy is 1.184 for a physical void anisotropy of 1.20.

This effect may be explained by treating the highly diluted ferrofluid as comprising clusters of magnetic particles suspended in a non-magnetic carrier fluid. In this scenario, the measuring field no longer ‘sees’ the ferrofluid as a homogeneous substance but as ‘pockets’ of susceptible nano-particles that interact with each other. It is likely that such an interaction plays a key role in reducing the effectiveness of the equivalent pore concept. Hence, a concentration or intrinsic susceptibility threshold may be reached below which the EPC method ceases to work reliably. From our measurements, this threshold seems to occur at

approximately 50% concentration (K_i = 1.09). However, a detailed mathematical analysis of such an interaction is beyond the scope of the current study.

The EPC method therefore appears to be highly effective at correcting pAMS data for the demagnetization effect at high concentrations but is considerably less effective at low concentrations. This concentration issue is important, however, because it is common practice to use diluted ferrofluid when making pAMS measurements on high porosity rocks (e.g. Benson et al., 2003; Benson, 2004). This is done in order to avoid very high susceptibilities in ferrofluid saturated pore space overloading sensitive susceptibility bridges built to measure the low susceptibilities of the dry rock matrix. We therefore tentatively suggest an empirical correction factor, based on the data of Figure 9, which may be used to correct EPC predicted anisotropy when using low concentration ferrofluid. The correction factor (β) is based on a double exponential fit to the EPC calculated void anisotropy data as a function of intrinsic susceptibility, and is given by: . When the EPC calculated void anisotropy is multiplied by β, for this particular void anisotropy of a/r = 1.2, it effectively corrects for the concentration error. Finally, Figure 10 shows how the value of β decreases as the intrinsic susceptibility of the ferrofluid increases.

Conclusions

We conclude that the equivalent pore concept methodology can be highly effective in calculating physical pore fabrics from measured pAMS data. However, a high concentration ferrofluid must be used for reliable results. Our results suggest that the most likely cause of the non-linear relation between the EPC calculated void geometry and the real, physical void geometry as a function of ferrofluid concentration arises from the non-linear relation between

the intrinsic and measured susceptibility of the fluid. As published, the EPC (Hrouda et al., 2000) does not adequately account for ferrofluid concentration. The concentration issue is serious, since it is common practice to use diluted ferrofluid when studying high porosity rocks in order to avoid overloading sensitive susceptibility bridges. We have therefore tentatively proposed an empirical correction factor, based on our experimental measurements, that takes account of the intrinsic susceptibility of ferrofluid of any concentration. However, we have only studied the concentration effect for a single void space geometry ($a/r = 1.2$), and a full appraisal of this problem may require a more systematic study of a range of void space geometries.

References

Benson, P.M., Meredith, P.G. and Platzman, E.S., 2003. Relating pore fabric geometry to elastic and permeability geometry in Crab Orchard sandstone: a laboratory study using magnetic ferrofluid, *Geophys. Res. Lett.*, **30(19)**, 1976, doi:10.1029/2003GL017929

Benson, P.M., 2004. *Experimental study of void space, permeability and elastic anisotropy in crustal rock under ambient and hydrostatic pressure*, Ph.D. thesis, University of London, London.

Benson, P. M., P. G. Meredith, E. S. Platzman, and R. E. White, 2005. Pore fabric shape anisotropy in porous sandstone and its relation to elastic and permeability anisotropy under isostatic pressure, *Int. Journal. Rock. Mech.,* **42**, 890-899, doi:10.1016/j.ijrmms.2005.05.003.

Collinson, D.W., 1983. *Methods in Rock Magnetism and Palaeomagnetism,* Chapman and Hall, London, 503pp.

Flinn, D., 1962. On folding during 3-D progressive deformation, *Q. J. Geol. Soc. Lond.*, **118**, 385-428.

Hrouda, F., 1982. Magnetic anisotropy of rocks and its application in geology and geophysics, *Geophys. Surv.*, **5,** 37–82.

Hrouda, F., Hanak, J. and Terzijski, I., 2000. The magnetic and pore fabrics of extruded and pressed ceramic models, *Geophys. J. Int.*, **142**, 941-947.

Jelinek, V., 1978. Statistical processing of anisotropy of magnetic susceptibility measured on groups of specimens, *Studia Geoph. Geod.*, **22**, 50-62.

Jones C. & Meredith P.G., 1998. An experimental study of elastic wave propagation anisotropy and permeability anisotropy in an illitic shale, In: Eurock '98, Rock Mechanics in Petroleum Engineering, Vol. 2, 307-313, SPE/ISRM 47369.

Lo, T-w, Coyner, K.B. and Toksoz, M.N., 1986. Experimental determination of elastic anisotropy of Berea sandstone, Chicopee shale, and Chelmsford granite, *Geophysics,* **51**, 164-171.

Louis, L., David, C., Metz, V., Robion, P., Menéndez, B., and Kissel, C., 2005. Microstructural control on the anisotropy of elastic and transport properties in undeformed sandstones. *Int. Journal. Rock. Mech.,* 42, *911-923,* doi:10.1016/j.ijrmms.2005.05.004.

Osborn, J.A., 1945. Demagnetising factors of the general ellipsoid, *Physical Review,* **67**, 345-357.

Pfleiderer, S. and Halls, H.C., 1990. Magnetic susceptibility anisotropy of rocks saturated with ferrofluid: a new method to study pore fabric? *Phys. Earth Plan. Int.,* **65**, 158-164

Pfleiderer, S., and Halls, H.C., 1993. Magnetic Pore Fabric Analysis: Verification through image autocorrelation. *J. Geophys. Res*., **98**, 4311-4316

Pfleiderer, S. and Halls, H.C., 1994. Magnetic pore fabric analysis: a rapid method for estimating permeability anisotropy, *Geophys. J. Int.,* **116**, 39-45.

Pfleiderer, S. and Kissel, C., 1994. Variation of pore fabric across a fold-thrust structure, *Geophys. Res. Lett.,* **21**, 2147-2150.

Porath, H., Stacey, F.D. and Cheam, A.S., 1966. The choice of specimen shape for magnetic anisotropy measurements on rocks. *Earth Plan. Sci. Lett*., **21,** 2147-2150.

Rasolofosaon, P.N.J. and Zinszner, B.E, 2002. Comparison between permeability anisotropy and elastic anisotropy of reservoir rocks, *Geophysics,* **67**, 230-240.

Stoner, E.C., 1945. The demagnetizing factors for ellipsoids, *Phil. Mag.,* Ser., 7, **36**, 803-821.

Tarling, D.H. and Hrouda, F., 1993. *The Magnetic Anisotropy of Rocks,* Chapman and Hall, London, 217pp.

Uyeda, S., Fuller, M.D., Belshe, J.C. and Girdler, R.W., 1963. Anisotropy of magnetic susceptibility of rocks and minerals, *J. Geophys. Res.,* **68**, 279-291.

Zhang, S. and Jin, J., 1996, *Computation of Special Functions*, Wiley & Sons, New York, 717 pp.

Figure Captions

Figure 1: Schematic visualization of a rock pore fabric before (top) and after (bottom) ferrofluid saturation.

Figure 2: Graphical representation of a susceptibility ellipsoid of principal susceptibility axis lengths $k_1>k_2>k_3$, and principal void space ellipsoid axis lengths a>b>c, relative to a general co-ordinate frame O_{xyz}. After Tarling and Hrouda (1993).

Figure 3: Flinn plots of: (left) EPC analysis applied to 50% concentration ferrofluid with an intrinsic susceptibility of 0.38; and (right) EPC analysis applied to 100% (undiluted) ferrofluid with an intrinsic susceptibility of 3.34.

Figure 4: Schematic views of the four 'special' void space fabric used in this study: (a) the cylinder representing a quasi-sphere, (b) the bedding-like fabric, (c) the capillary-like fabric, and (d) the crack-like fabric.

Figure 5: Schematic views of the seven different quasi-spheroidal void space fabrics used in this study: (a) a sphere, (b to d) prolate quasi-spheroids of increasing anisotropy, and (e to g) oblate quasi-spheroids of increasing anisotropy.

Figure 6: A: Flinn plot (lineation vs. foliation) of pAMS results for all the synthetic fabrics used in this study. Note particularly the results for the 'special' fabrics. The capillary-like fabric is highly prolate, with high lineation and zero foliation, the crack-like fabric is highly oblate, with high foliation and zero lineation, and the bedding-like fabric both high lineation and high foliation.
B: Expanded view of the Flinn plot view of Figure 5A. Note that the sphere and the cylindrical quasi-sphere both plot close to the origin, as expected. The quasi-ellipsoidal cavities, however, show a decreasing foliation and increasing lineation with increasing a/r ratio.

Figure 7: Measured pAMS void anisotropy (solid circles) and EPC calculated void anisotropy (solid triangles) plotted against known physical void anisotropy for quasi-spheroidal samples. Solid lines are least squares fits to the data, and the dashed illustrates perfect correlation. A ferrofluid concentration of 50% was used in all cases, with $K_i = 1.09$.

Figure 8: A: The non-linear relationship between measured susceptibility (K_m) and intrinsic susceptibility (K_i) of a sphere for K_i up to 5, as calculated from equation (2). B: The relationship between calculated lineation (L) and intrinsic susceptibility (K_i) for three different anisotropic pore geometries (a>b>c), as calculated from equations 1, 3, 4 and 5. Arrows illustrate the ferrofluid concentration used in this study.

Figure 9: Plot of measured pAMS lineation (L_M) and EPC calculated void anisotropy against intrinsic susceptibility (K_i) for a known physical void anisotropy of 1.20. Magnetic lineation increases linearly with increasing K_i, but EPC calculated anisotropy increases very non-linearly with K_i, becoming asymptotic a physical void anisotropy of 1.184 at high intrinsic susceptibility.

Figure 10: Empirical correction factor (β) as a function of ferrofluid intrinsic susceptibility (K_i). The correction factor decreases very rapidly with increasing intrinsic susceptibility, becoming asymptotic to 1.139 at high susceptibility.

Figure 1:

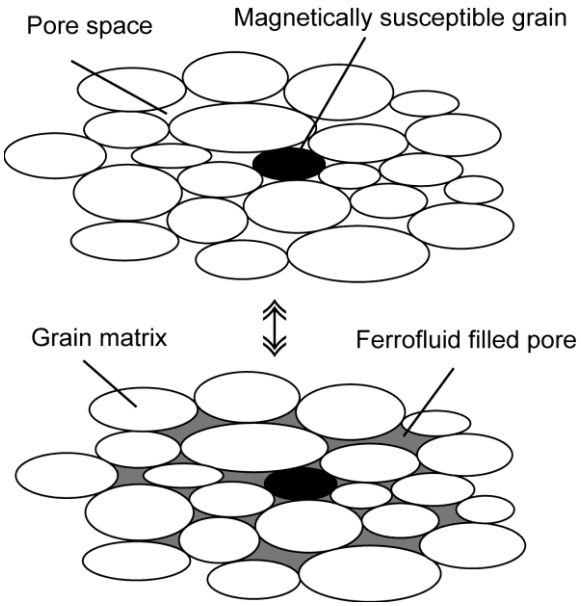

Figure 2:

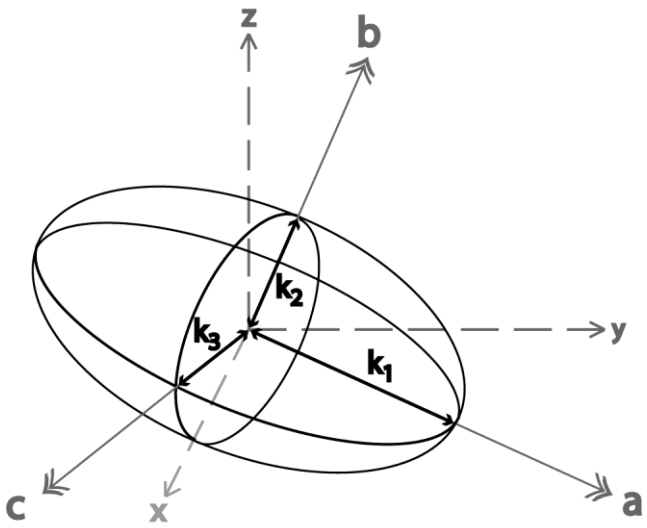

Figure 3:

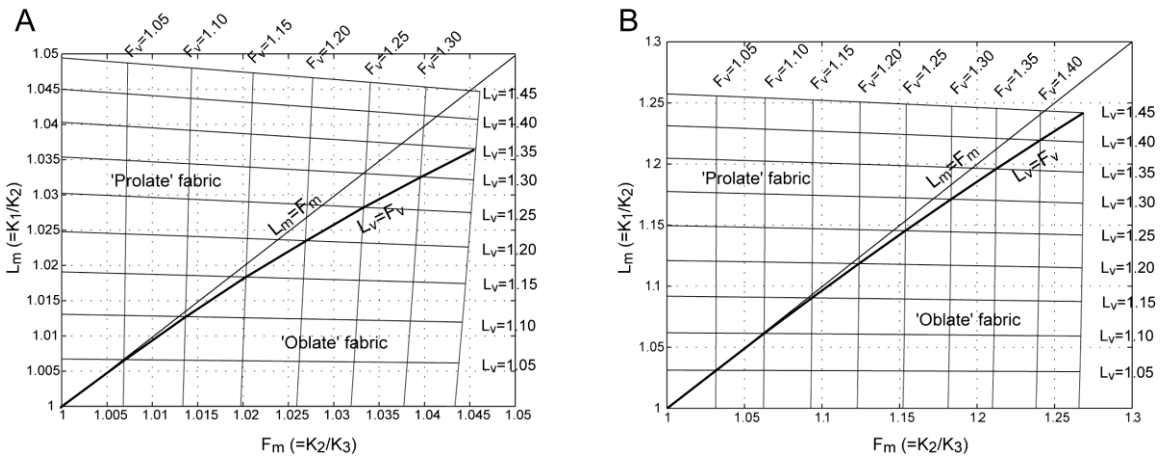

Figure 4, 5:

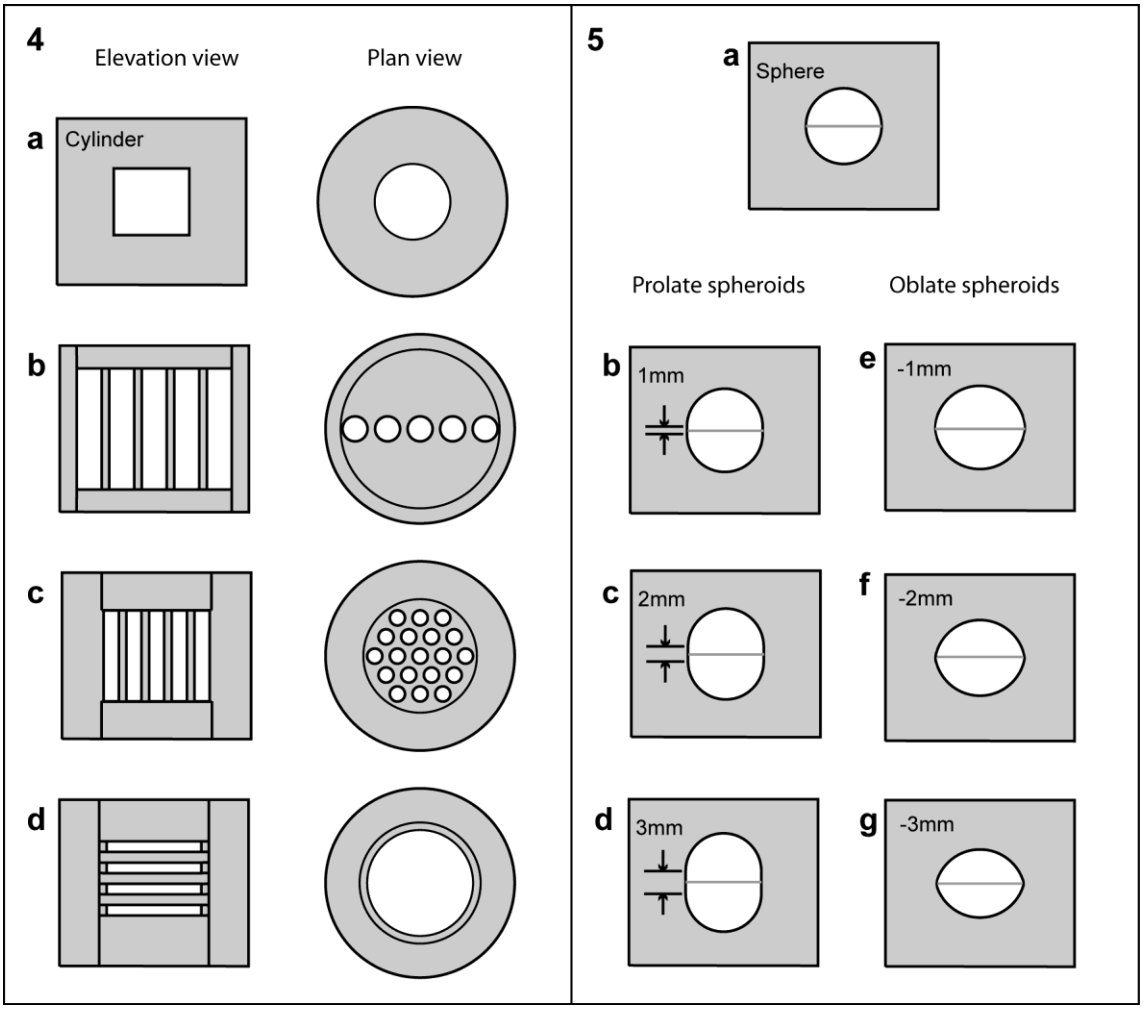

Figure 6:

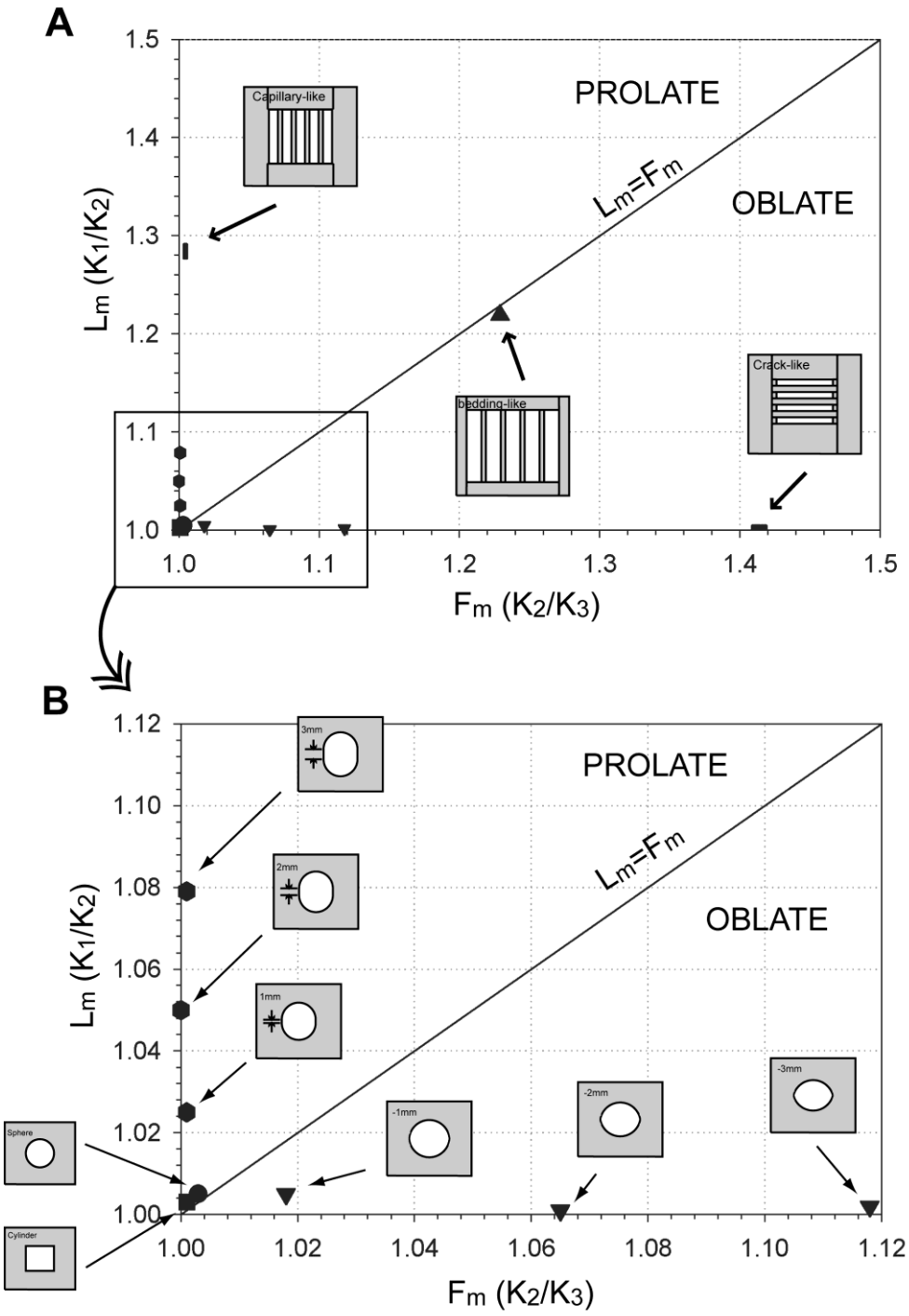
A
PROLATE
OBLATE
Lm=Fm
Capillary-like
bedding-like
Crack-like
Lm (K1/K2)
Fm (K2/K3)
1.0
1.1
1.2
1.3
1.4
1.5
B
PROLATE
OBLATE
Lm=Fm
3mm
2mm
1mm
Sphere
Cylinder
-1mm
-2mm
-3mm
Lm (K1/K2)
Fm (K2/K3)
1.00
1.02
1.04
1.06
1.08
1.10
1.12

Figure 7:

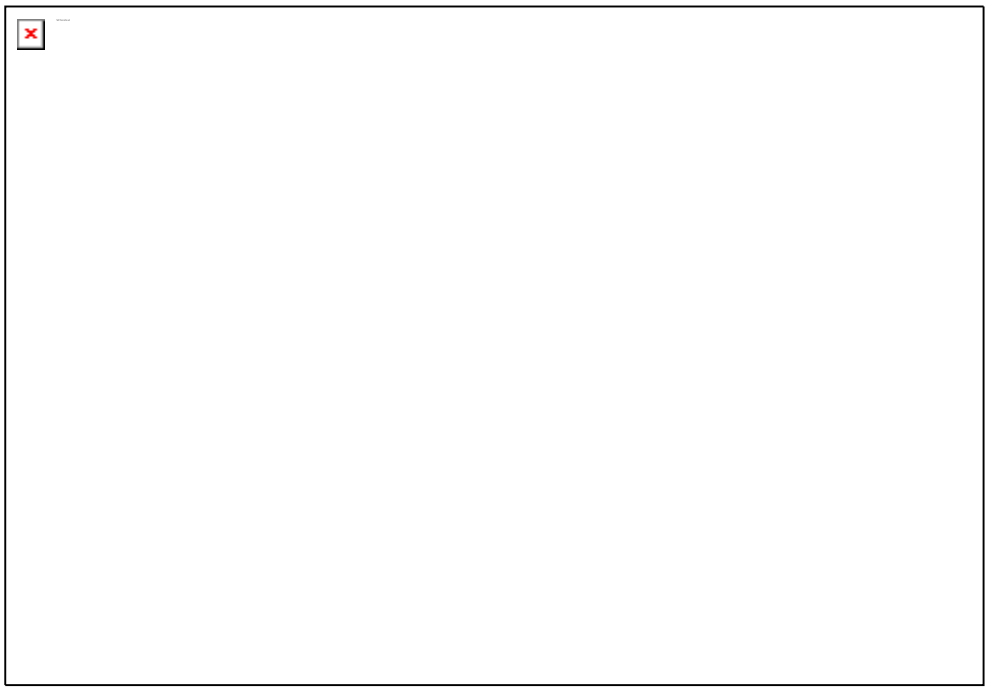

Figure 8:

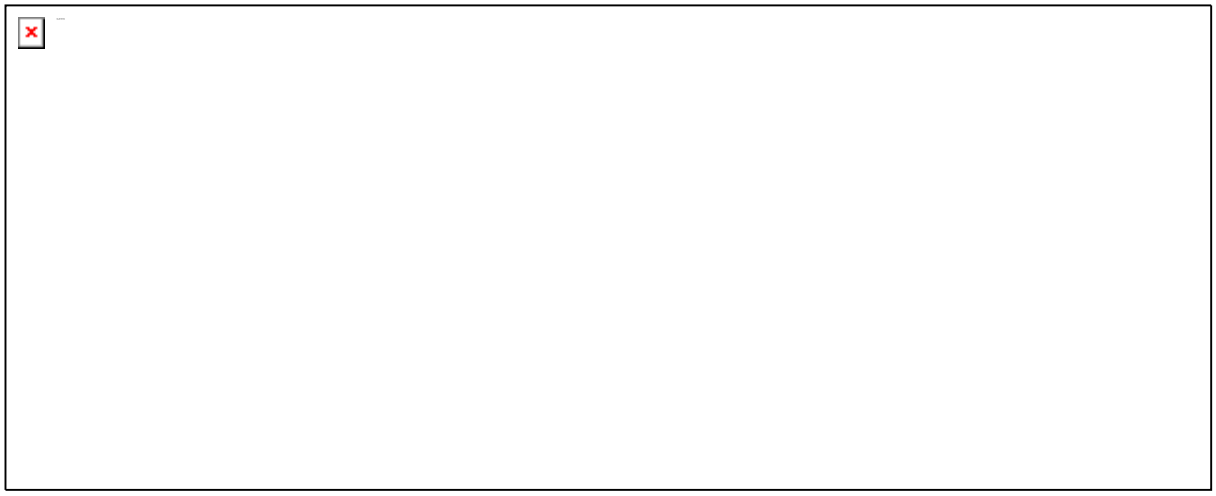

Figure 9:

Figure 10: